IEEE Access
Multidisciplinary | Rapid Review | Open Access Journal

Received January 21, 2021, accepted February 5, 2021, date of publication February 10, 2021, date of current version February 18, 2021.

Digital Object Identifier 10.1109/ACCESS.2021.3058257

Workspace Derivation of Arthroscope Using Morphological Data and Standard Portal Placement Method for Shoulder Arthroscopy

CHANG-KYUN KIM[1,2], JOONHWAN KIM[1], DONGJUN PARK[3], AND DONG-SOO KWON[1,2], (Senior Member, IEEE)

[1]Division of Mechanical Engineering, School of Mechanical, Aerospace and Systems Engineering, Korea Advanced Institute of Science and Technology, Daejeon 34141, South Korea
[2]EasyEndo Surgical Inc., Daejeon 34051, South Korea
[3]Asan Medical Center, Department of Orthopedic Surgery, University of Ulsan College of Medicine, Seoul 05505, Republic of Korea

Corresponding author: Dong-Soo Kwon (kwonds@kaist.ac.kr)

This work was supported in part by the National Research Foundation of Korea through the Framework of International Cooperation Program under Grant 2019K2A9A2A06025429 and Grant FY2019, in part by the Korea Medical Device Development Fund grant funded by the Korea Government (the Ministry of Science and ICT, the Ministry of Trade, Industry and Energy, the Ministry of Health & Welfare, Republic of Korea, the Ministry of Food and Drug Safety) under Project 202012D18.

ABSTRACT Robotic arthroscopy is a potential alternative surgery method because the use of robotic arthroscope manipulators could ensure a constant quality of view that would enhance the workflow of the operator. To achieve this advancement, a workspace derivation for the movement of the arthroscope in the human joint is needed. There is a key requirement for workspace derivation of the arthroscope: the workspace should incorporate all the essential observation sites to ensure a suitable field of view during an arthroscopic surgery for various patients. The workspace could be delineated via workspace measurements on various patients or cadavers; however, this would be an arduous process. Herein, we propose a workspace derivation using morphological measurement data of various human shoulder joints for arthroscopic rotator cuff repair, which is a typical operation in arthroscopy. First, we present the geometrical modeling of the human shoulder joint using morphological parameters and standard portal placement methods. Second, the morphological measurement data of the human joint are substituted for the parameters to determine the workspace required for arthroscopic rotator cuff repair. As a result, we obtain the location of each portal and the workspace of the arthroscope via the portals that incorporate all the essential observation sites. We verify the derived workspace through several cadaveric tests. For all the experimental results, it was confirmed that the 95^{th} percentile of the range of motion was formed within the workspace obtained using the proposed method. The results verify that the proposed method is feasible for arthroscopy.

INDEX TERMS Medical robotics, endoscopes, surgery, motion measurement, surgical instruments.

I. INTRODUCTION

Arthroscopy is a substitute for open surgery in orthopedics, and its types are gradually expanding. Among them, shoulder arthroscopy accounts for a large proportion of surgical operations. Rotator cuff repair is a typical operation in shoulder arthroscopy, in which the surgeon must perform a highly complex procedure in the shoulder joint of the patient. Therefore, significant labor is needed to utilize various surgical instruments, which means that the help of assistants is required.

In such a surgery, the operator performs various suture procedures, whereas the assistants primarily manipulate the arthroscope, which enables the field of view of the operating area to be secured. There are various difficulties associated with this process, such as unclear orientation due to the fulcrum motion and screen shaking caused by hand tremors [1]. Furthermore, there is a limitation that the quality of surgery varies with the ability of the surgical assistants. If a robotic arthroscope manipulator is employed, the aforementioned problems can be solved through intuitive, smooth, and stable movement of the robotic arm. Therefore, a robotic arthroscope manipulator that could secure a constant quality

The associate editor coordinating the review of this manuscript and approving it for publication was Zhong Wu.

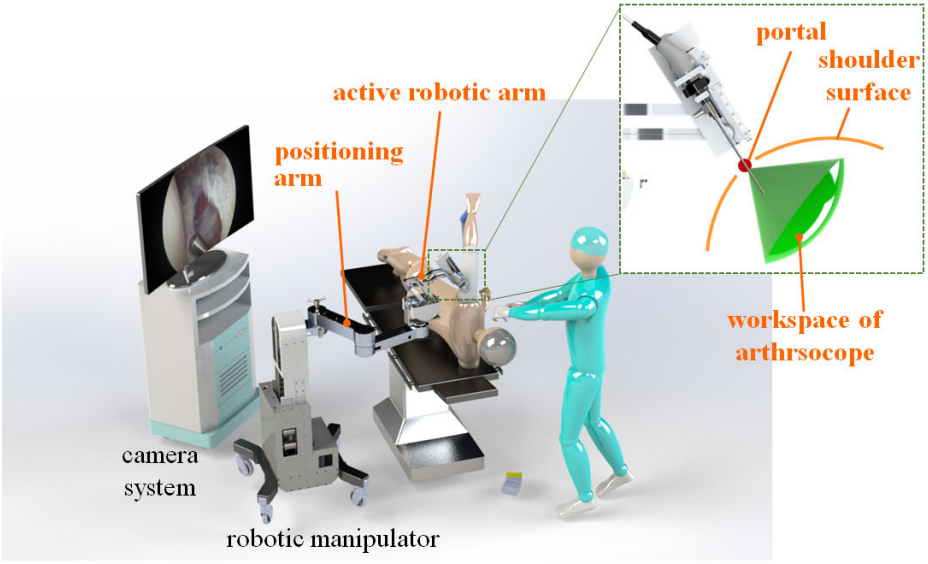

FIGURE 1. System layout of shoulder arthroscopy using robotic arthroscope manipulator.

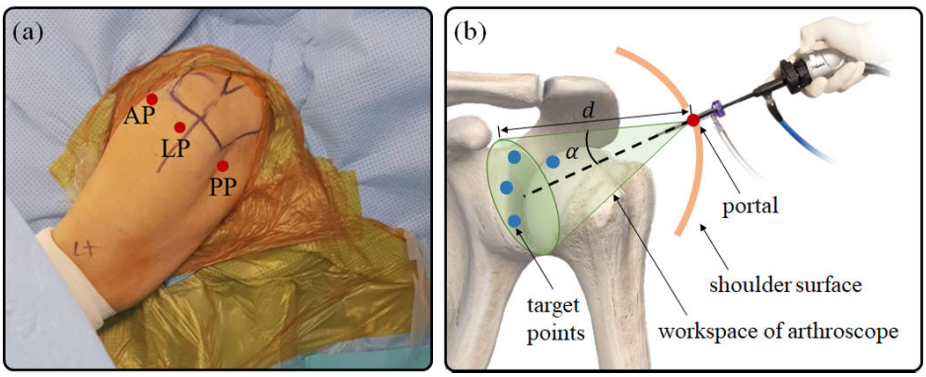

FIGURE 2. (a) Three basic portals for shoulder arthroscopy, (b) shape and parameters of workspace of arthroscope.

of view would help increase the stability of the procedure of the operator.

In the laparoscopic field, robotic camera manipulators have been actively investigated [2]–[10]. They utilized the following laparoscope control method not to increase the operator's workload excessively as well as to ensure safe surgical assistance: autonomous tool tracking algorithm, a small joystick that is attachable to a surgical instrument, system that make laparoscope imitate operator's head motion. However, a robotic arthroscope manipulator is yet to be developed in the orthopedic field. A robotic arthroscope manipulator can be designed as shown in Fig. 1. To design a robotic arthroscope manipulator, a workspace derivation of the arthroscope's movement in the affected area must be performed first for the following reasons. First, the workspace analysis results can be used to design a robot that is optimized for the workspace of the target operation. For example, the active robotic arm can be optimized according to the range of motion around the portal [11]. Furthermore, the link length of the positioning arm can be optimized according to the location of the portal [12]. Second, the initial position of the robot base point can be optimized for the workspace of the target operation. If the initial positioning of the base point is not properly performed, the end effector of the robot cannot reach the target point during surgery, which would necessitate repositioning. Therefore, to limit the operation time, the initial positioning of the base point for the target workspace is important, and a considerable amount of research has been conducted in this regard [13], [14].

For workspace derivation, Cao, C., et al analyzed the motion of a surgical instrument by taking videos of 1 expert and 5 novices while they do laparoscopic animal tests [15]. Person, J. G., et al proposed an automatic system that measures the motion of the operator during laparoscopy by using a Polaris position sensor and video camera [16]. Riener, R., *et al.* analyzed the motion of 2 surgeons during 6 cases of

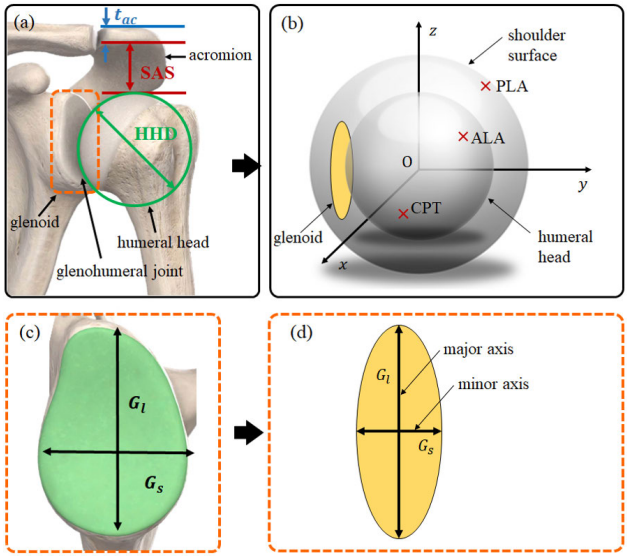

FIGURE 3. (a) Shoulder anatomy, (b) geometric model of shoulder anatomy, (c) glenoid, and (d) geometric model of glenoid.

laparoscopy by using an electromagnetic tracking system [17]. Jacob Rosen *et al.* developed a passive robotic system to analyze surgical instrument tip position in laparoscopy [18]. In an arthroscopy study, 5 inertial sensors (inertial measurement unit (IMU) sensors) were attached to the operator's upper limb to analyze the workspace [19]. However, all the aforementioned studies have the limitation that data were obtained only for very few patients or animals; workspace analysis for large numbers of patients has not been actively explored. Acquiring data from numerous patients or animals is a very arduous process. Therefore, in this study, we propose a workspace derivation method using morphological data of various shoulder joints. The proposed method has the advantage of being able to derive reliable workspace without time-consuming and expensive experiments to acquire actual measurement data.

To ensure field of view during arthroscopic surgery, the arthroscope's workspace should include all essential observation sites for various patients. The workspace of the arthroscope in patients' shoulder joints will vary greatly depending on the size of the patient's body and the size of the bone. Workspace measurements on various patients or cadavers will be time-consuming and expensive. In this study, we propose a workspace derivation method for arthroscopic rotator cuff repair using morphological measurement data of various human shoulder joints. Because the morphological data contain information on a wide variety of shoulder joints, a workspace of the arthroscope that incorporates various shoulder joints can be derived without an arduous process. Furthermore, the derived model of the shoulder joint can be utilized to derive the workspace for not only rotator cuff repair but also various shoulder arthroscopies. The proposed method can be used in various orthopedic applications that involve large amounts of morphological data, such as knee joints and hip joints.

In Section II, an overall description of the surgery and desired workspace is provided. Section III presents the geometrical modeling of the human shoulder joint using morphological parameters. In addition, the three-dimensional positions of important landmarks are derived using morphological measurements. Deriving the positions of landmarks is necessary because they must be observed during surgery or serve as a criterion for the locations of basic portals. Based on this information, the positions of the basic portals where the arthroscope is inserted into the shoulder are determined using the standard portal placement method. With the geometric relationship between the portals and the landmarks that should be observed during the surgery, Section IV describes the delineation of a conical workspace that the arthroscope should reach during the surgery. In Section V, for evaluation, the workspace of an arthroscope during arthroscopic examination and rotator cuff repair is measured via a cadaveric test and compared with the theoretical workspace. Finally, a discussion of the results and the conclusions of this study are presented in Sections VI and VII, respectively.

II. SURGICAL PROCESS AND DEFINITION OF WORKSPACE

As shown in Fig. 2 (a), three basic portals are used in arthroscopy: anterior portal (AP), posterior portal (PP), and lateral portal (LP). During all shoulder arthroscopies, the surgeon performs arthroscopic examination of the shoulder joint by inserting an arthroscope into the PP. In this process, other surgical instruments are not inserted, and the surgeon observes the glenohumeral joint (Fig. 3 (a)) using the arthroscope. During rotator cuff repair, the arthroscope is inserted into the LP to secure the site of the subacromial space (*SAS* in Fig. 3 (a)) of the shoulder joint. Surgical instruments, such as radiofrequency ablation devices, shavers, and suture lassos, are inserted into the remaining two portals. The surgeon uses the surgical instruments to affix the torn tendon to the surface of the humeral head (spherical head of humerus in Fig. 3 (a)).

As depicted in Fig. 2 (b), during the surgical task discussed in the previous paragraph, the arthroscope performs a fulcrum motion around the portal. Therefore, the workspace of the arthroscope can be expressed as a conical shape with the portal location as the vertex point. The conical workspace is represented using half of the vertex angle and the slant height (α and d in Fig. 2 (b), respectively), where α represents the angle between the longitudinal vector of the arthroscope and the axis of rotation of the conical workspace, and d indicates the translationally moved distance required to reach the target point from the portal location. If the arthroscope has a conical workspace with α and d that can contain all the target points, the operator will be able to observe all the desired points for shoulder arthroscopy. Thus, we will find α and d values of the arthroscope's conical workspace at LP and PP.

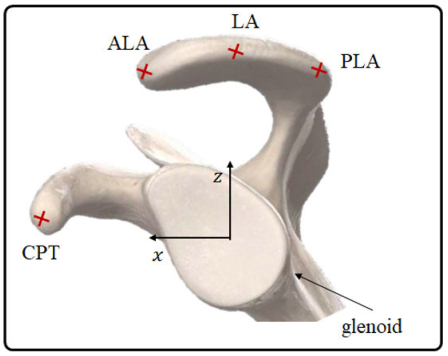

FIGURE 4. Scapula that contains several points, such as anterolateral tip of acromion (ALA), lateral tip of acromion (LA), posterolateral tip of acromion (PLA), and coracoid process tip (CPT).

III. GEOMETRIC MODEL OF SHOULDER ANATOMY

In this section, we describe the workspace of an arthroscope in shoulder arthroscopy. The geometric model that corresponds to the shoulder joint anatomy is described in the Cartesian coordinate system. Based on the derived model, we present the derivation of the locations of the anatomic landmarks of the human shoulder joint and three basic portals.

A. LOCATION DERIVATION OF ANATOMIC LANDMARKS IN SHOULDER JOINT

In this section, the locations of the landmarks, such as the anterolateral tip of acromion (ALA), lateral tip of acromion (LA), and posterolateral tip of acromion (PLA), and coracoid process tip (CPT) are derived to identify the positions of portals. The geometric model is derived based on the left shoulder. The model for the right shoulder can also be easily derived by interchanging the left and right shoulders. Fig. 3 (a) displays the shoulder anatomy. The humeral head can be assumed to be a sphere with the center at origin O, as shown in Fig. 3 (b), and a diameter equal to the humeral head diameter (*HHD* in Fig. 3) [20]. Thus, the surface of the humeral head can be derived as follows:

$$x^2 + y^2 + z^2 = \left(\frac{HHD}{2}\right)^2 \tag{1}$$

The shoulder surface can also be assumed to be a sphere with the center at origin O and a radius that is the sum of $HHD/2$, the *SAS* [21], and the thickness of the acromion (t_{ac}) [22], as depicted in Fig. 3 (a) and (b). Therefore, the surface of the human shoulder can be assumed to be

$$x^2 + y^2 + z^2 = r_s^2 \tag{2}$$

where $r_s = \frac{HHD}{2} + SAS + t_{ac}$. Fig. 3 (c) depicts a glenoid. G_l and G_s denote the lengths of the longer axis and the shorter axis, respectively, of the glenoid [23]. A glenoid can be assumed to be an ellipse with a major axis of length G_l and a minor axis of length G_s, as shown in Fig. 3 (d). The glenoid is attached to the humeral head surface and can be modeled as an ellipse on a plane perpendicular to the y axis (Fig. 3 (b));

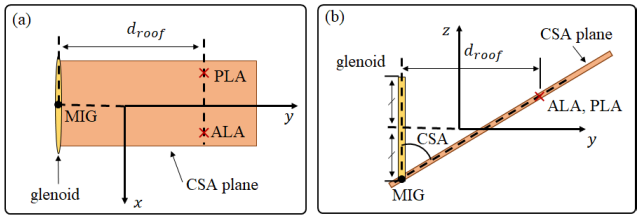

FIGURE 5. Location of ALA and PLA (a) top view and (b) front view.

therefore, it can be derived as follows:

$$\left(\frac{x}{G_s}\right)^2 + \left(\frac{z}{G_l}\right)^2 \le \frac{1}{4}, \quad y = -\frac{HHD}{2} \tag{3}$$

The basic portals of shoulder arthroscopy—AP, PP, and LP—can be located based on the lateral edge of the acromion and the CPT. Therefore, we determine the locations of the ALA and PLA (Fig. 4). The critical shoulder angle (*CSA*) plane (Fig. 5 (a)) that is perpendicular to the yz plane, including the most inferior point of the glenoid (MIG in Fig. 5) and the lateral edge of the acromion, is expressed as follows:

$$\left(\frac{G_l}{2} + z\right) sin(CSA) = \left(\frac{HHD}{2} + y\right) cos(CSA) \tag{4}$$

In (4), the *CSA* is the angle between the *CSA* plane and the glenoid [24]. The ALA and PLA are located at a point d_{roof} far from the glenoid in the y direction [24]. In this case, the plane away from the glenoid in the y direction by d_{roof} is expressed as follows using (3):

$$y = -\frac{HHD}{2} + d_{roof} \tag{5}$$

Because the ALA and PLA are also located on the shoulder surface, the positions of the former (P_{ALA}) and the latter (P_{PLA}) can be expressed as follows using (2), (4), and (5):

$$P_{ALA} = \begin{bmatrix} \sqrt{r_s^2 - W^2 - H^2} \\ W \\ H \end{bmatrix} \tag{6}$$

$$P_{PLA} = \begin{bmatrix} -\sqrt{r_s^2 - W^2 - H^2} \\ W \\ H \end{bmatrix} \tag{7}$$

where $W = -\frac{HHD}{2} + d_{roof}$, $H = \frac{2d_{roof}\,cos(CSA) - G_l sin(CSA)}{2sin(CSA)}$.

The LA can be defined as the middle point of the ALA and PLA, as depicted in Fig. 6 (a). Assuming that the acromial arch is on a plane perpendicular to the y axis as shown in Fig. 6 (b), the position of the LA (P_{LA}) can be expressed using (6) and (7) as follows.

$$P_{LA} = \begin{bmatrix} 0 \\ W \\ \sqrt{r_s^2 - W^2} \end{bmatrix} \tag{8}$$

The CPT (Fig. 4 and 7) is separated from the glenoid plane by the CP (Fig. 7) in the y direction. The CPT is also d_{cg} away from the uppermost point of the glenoid in the z direction [25].

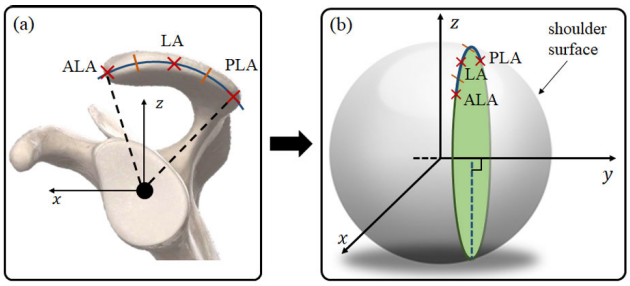

FIGURE 6. (a) Acromial arch (b) geometric model of ALA, PLA, and LA.

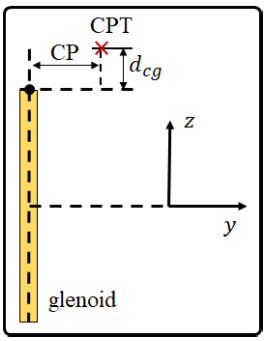

FIGURE 7. Location of CPT.

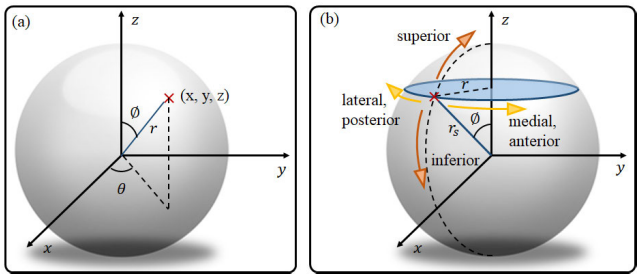

FIGURE 8. (a) Spherical coordinate and (b) movement direction in spherical coordinates of left shoulder.

Therefore, the location of the CPT (P_{CPT}) can be expressed using (3).

$$P_{CPT} = \begin{bmatrix} \sqrt{r_s^2 - y_c^2 - z_c^2} \\ y_c \\ z_c \end{bmatrix} \tag{9}$$

where $y_c = -\frac{HHD}{2} + CP$ and $z_c = d_{cg} + \frac{G_l}{2}$.

B. LOCATION DERIVATION OF THREE BASIC PORTALS FOR SHOULDER ARTHROSCOPY

Because the portals are positioned on the surface of the shoulder, which was previously assumed to be a sphere, their locations can be derived in spherical coordinates. As shown in Fig. 8 (a), Cartesian coordinates can be converted into spherical coordinates as follows:

$$P = \begin{bmatrix} r \\ \theta \\ \phi \end{bmatrix} = \begin{bmatrix} \sqrt{x^2 + y^2 + z^2} \\ tan^{-1}\left(\frac{y}{x}\right) \\ cos^{-1}\left(\frac{z}{r}\right) \end{bmatrix} \tag{10}$$

The AP is located lateral to the halfway point between the CPT and the ALA [26]. Specifically, the AP is located at the midpoint of the CPT and P_{ALA} in the spherical coordinate system. The location of the AP (P_{AP}) can be derived using (6), (9), and (10) as follows:

$$P_{AP} = \begin{bmatrix} r_{AP} \\ \theta_{AP} \\ \phi_{AP} \end{bmatrix} = \begin{bmatrix} r_s \\ \frac{1}{2}\left(tan^{-1}\left(\frac{y_C}{\sqrt{r_s^2 - y_C^2 - z_C^2}}\right) - tan^{-1}\left(\frac{-W}{\sqrt{r_s^2 - H^2 - W^2}}\right)\right) \\ \frac{1}{2}\left(tan^{-1}\left(\frac{\sqrt{r_s^2 - z_C^2}}{z_C}\right) - tan^{-1}\left(\frac{-\sqrt{r_s^2 - H^2}}{H}\right)\right) \end{bmatrix} \tag{11}$$

The PP is located 1cm medial and 1.5–3cm inferior to the PLA [26]. As presented in Fig. 8 (b), the radius of the circle that is on the shoulder surface and the plane perpendicular to the z-axis can be expressed as follows:

$$r = r_s sin\phi \tag{12}$$

The distance (l_{ml}) movement in the medial or lateral direction is equal to the distance passed when the point moves on this circle. Therefore, the change in angle θ ($\Delta\theta$) in the spherical coordinate system when a point moves in the medial or lateral direction can be derived as follows:

$$\Delta\theta = \frac{l_{ml}}{r_s sin\phi} \tag{13}$$

The change in angle θ during a medial or lateral directional movement from the PLA can be expressed using (7) and (13) as follows:

$$\Delta\theta_{PLA} = \frac{l_{Pml}}{\sqrt{r_s^2 - H^2}} \tag{14}$$

where l_{Pml} represents the medially or laterally moved distance from the PLA. Similarly, the distance l_{si} moving in the superior or inferior direction is equal to the distance that the point passes while changes of ϕ occur in the spherical coordinate system. Therefore, the change of ϕ in a superior or inferior directional movement from the PLA can be derived as

$$\Delta\phi_{PLA} = \frac{l_{Psi}}{r_s} \tag{15}$$

where l_{Psi} represents the superior or inferior directional moved distance from the PLA. The position of PP, P_{PP}, can be calculated using (7), (14), and (15):

$$P_{PP} = \begin{bmatrix} r_{PP} \\ \theta_{PP} \\ \phi_{PP} \end{bmatrix} = \begin{bmatrix} r_s \\ tan^{-1}\left(\frac{-W}{\sqrt{r_s^2 - H^2 - W^2}}\right) + \Delta\theta_{PLA} \\ tan^{-1}\left(\sqrt{\frac{r_s^2}{H^2} - 1}\right) + \Delta\phi_{PLA} \end{bmatrix} \tag{16}$$

TABLE 1. Direction mapping between spherical coordinates and human shoulder (*M, medial; L, lateral; A, anterior; P, posterior; S, superior; I, inferior direction.).

parameter	sign	right shoulder		left shoulder	
		$\theta > 3\pi/2$	$\theta < 3\pi/2$	$\theta > \pi/2$	$\theta < \pi/2$
θ	+	M, A	L, A	M, P	L, P
	-	L, P	M, P	L, A	M, A
ϕ	+	S			
	-	I			

TABLE 2. Morphological data of human shoulder.

morphological data	sample size	results	reference
HHD [mm]	237	45.7±3.2	[20]
SAS [mm]	175	9.7±1.5	[21]
t_{ac} [mm]	160	9.1±2.7	[22]
G_l [mm]	264	35.7±2.9	[23]
G_s [mm]		26.2±2.7	
CSA [°]	70	34.5±4.3	[24]
d_{roof} [mm]		33.7±4.1	
CP [mm]	204	14.6±2.0	[25]
d_{cg} [mm]		7.1±1.2	

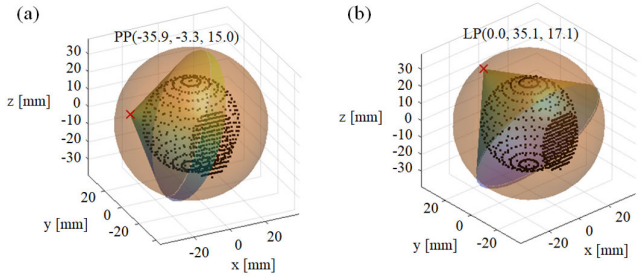

FIGURE 9. Derived conical workspace that incorporates target landmarks when arthroscope is inserted through (a) posterior portal and (b) lateral portal.

From (16), the signs preceding $\Delta\theta_{PLA}$ and $\Delta\phi_{PLA}$ can be determined as listed in TABLE 1. For example, in the PP of the left shoulder, the medial directional $\Delta\theta_{PLA}$ has the (+) sign because θ of P_{PP} is larger than $\pi/2$. The LP is located 3cm laterally away from the LA [26]. Similar to (15), if a distance is moved in the inferior or superior direction from the LA, l_{Lsi}, the angle $\Delta\phi_{LA}$ moved in the spherical coordinate system, can be expressed as follows:

$$\Delta\phi_{LA} = \frac{l_{Lsi}}{r_s} \tag{17}$$

The location of the LP, P_{LP}, can be expressed using (8), (10), and (17):

$$P_{LP} = \begin{bmatrix} r_{LP} \\ \theta_{LP} \\ \phi_{LP} \end{bmatrix} = \begin{bmatrix} r_{LA} \\ \theta_{LA} \\ \phi_{LA} + \Delta\phi_{LA} \end{bmatrix} = \begin{bmatrix} r_s \\ \frac{\pi}{2} \\ \frac{W}{\sqrt{r_s^2 - W^2}} + \frac{l_{Lsi}}{r_s} \end{bmatrix} \tag{18}$$

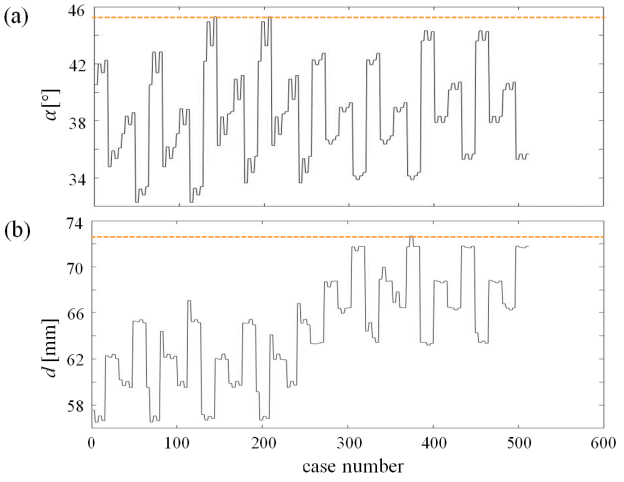

FIGURE 10. (a) Maximum angle between the arthroscope and normal vector of PP; (b) maximum translationally moved length of arthroscope end tip from PP.

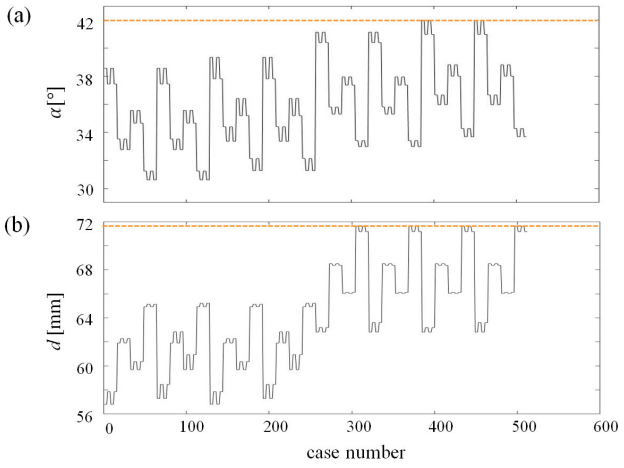

FIGURE 11. (a) Maximum angle between arthroscope and normal vector of LP; (b) maximum translationally moved length of arthroscope end tip from LP.

IV. WORKSPACE DERIVATION OF ARTHROSCOPE USING MORPHOLOGICAL DATA

In this section, morphological data (TABLE 2) are substituted for the parameters of the anatomical landmarks of the shoulder joint and portal placement, which were previously obtained to derive the workspace of the arthroscope. By substituting both the $\bar{x} - s$ and $\bar{x} + s$ of the morphological data into each parameter, the workspace of the arthroscope that contains the shoulder joint landmarks of various patients can be obtained (where $\bar{x}$ and s represent the mean value and the standard deviation of the morphological data, respectively).

Before arthroscopic rotator cuff repair, the surgeon conducts an arthroscopic examination through the PP with an arthroscope. Subsequently, he/she obserfves the SAS through the LP. Therefore, the workspace of the arthroscope for each case where the PP and LP are employed is derived.

The glenohumeral joint and periphery of the humeral head should be observed through the PP, during an arthroscopic

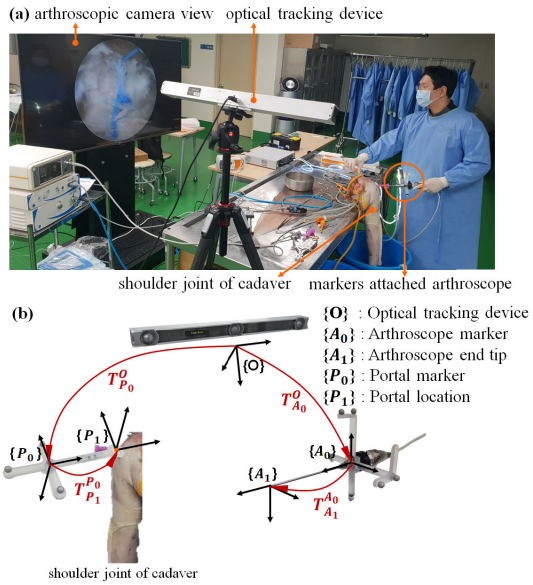

FIGURE 12. (a) Cadaveric experimental set-up for obtaining workspace of arthroscope; (b) transformation matrices among coordinates.

TABLE 3. Maximum α and d of conical workspace of arthroscope for arthroscopic examination and rotator cuff repair surgery.

portal location	maximum α	maximum d
PP	45.3	72.7
LP	42.0	71.6

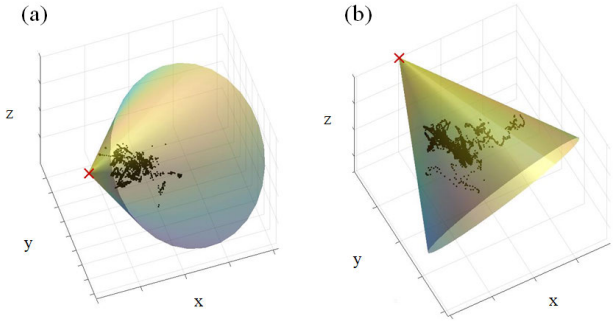

FIGURE 13. End tip position data of arthroscope and conical workspace that contains the points when arthroscope is inserted through (a) PP and (b) LP.

examination [27]. Furthermore, when performing rotator cuff repair, the arthroscope should observe the SAS around the humeral head through the LP. The rotator cuff tendon is located on the humeral head and can contract near the glenoid when a tear occurs [28]. Therefore, the workspace of the arthroscope should be able to contain the glenoid and humeral head through the PP. Thus, the workspace of the arthroscope can be represented as a conical shape that includes the humeral head and glenoid with the vertex point on the PP. The conical workspace is shown in Fig. 9 (a), and the red x mark represents the location of the PP. When substituting the $\bar{x} - s$ and $\bar{x} + s$ in TABLE 2 into each parameter in (1), (3), and (16), a total of 2^9 workspaces can be obtained, and the maximum α and d are presented in Fig. 10. The maximum values of α and d are 45.3°and 72.7 mm, respectively, which are indicated by orange dashed lines.

The arthroscope should observe the SAS around the humeral head through the LP when performing rotator cuff repair. Therefore, the arthroscope should be able to observe from the humeral head to the glenoid. Specifically, the workspace of the arthroscope can be expressed as a conical space that contains the humeral head and glenoid and has its vertex on the LP. The conical workspace is shown in Fig. 9 (b), and the red x mark represents the location of the LP. When substituting the $\bar{x} - s$ and $\bar{x} + s$ values in Table 2 into each of parameters (1), (3), and (18), a total of 2^9 workspaces can be obtained, as shown in the previous case. The results are shown in Fig. 11. The maximum values of α and d are 42.0°and 71.6mm, respectively, which are indicated by orange dashed lines.

TABLE 3 lists the maximum α and d of the workspace of the arthroscope in the PP and LP. During arthroscopic examination and rotator cuff repair, the arthroscope will move in a conical workspace with half of the vertex angle of 45.3° and a slant height of 72.7mm centered on the PP location. In addition, during rotator cuff repair, the arthroscope will move in a conical workspace with half of the vertex angle of 42.0° and a slant height of 71.6mm centered on the LP location. Because these results are calculated considering the morphological data of various patients, the derived workspace of the arthroscope with the proposed method represents various shoulder joints.

V. FEASIBILITY EVALUATION OF DERIVED WORKSPACE

To determine if the workspace of the arthroscope obtained, as described in Section IV, was actually feasible, an experiment was setup, as presented in Fig. 12 (a). One left shoulder of the cadaver was fixed in the beach chair posture. The position and rotation information of the portals and arthroscope were recorded using a 6-DOF optical tracking device (V120: Trio, NaturalPoint, Inc. DBA OptiTrack, US) and markers. The coordinate system of the experimental setup was established as shown in Fig. 12 (b). Markers were attached to the arthroscope and portal, and their 6-DOF motions were recorded. The transformation matrices from optical tracking device coordinate O to arthroscope marker coordinate A_0 and portal marker coordinate P_0 ($T^O_{A_0}$, and $T^O_{P_0}$, respectively) were converted to quaternions using optical motion capture software (Motive, NaturalPoint, Inc. DBA OptiTrack, US). In addition, the transformation matrix from portal marker coordinate to portal location coordinate ($T^{P_0}_{P_1}$) and that from arthroscope marker coordinate to arthroscope end tip coordinate ($T^{A_0}_{A_1}$) are described in TABLE 4. A total of two surgeons performed arthroscopic examinations and three surgeons performed rotator cuff repairs three times each, using an arthroscopic camera system ($Synergy^{UHD4}$ imaging platform, ARTHREX, USA) and arthroscopic instruments

TABLE 4. Transformation matrices to portal and arthroscope coordinates from each set of marker coordinates.

transformation matrix from portal marker to portal loaction, $T_{P_1}^{P_0}$				
	a_{i-1}	α_{i-1}	d_i	θ_i
1	0	$\pi/2$	160mm	0
transformation matrix from arthroscope marker to arthroscope end tip, $T_{A_1}^{A_0}$				
	a_{i-1}	α_{i-1}	d_i	θ_i
1	0	$\pi/2$	196mm	0

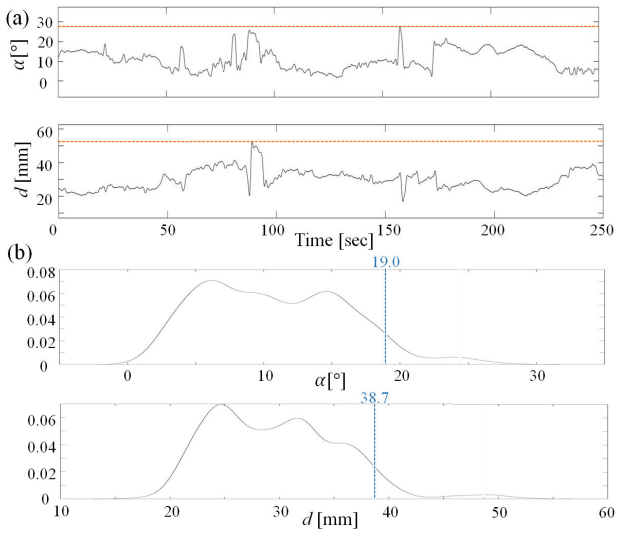

FIGURE 14. (a) α and d in time domain, (b) probability density of α and d during arthroscopic examination through PP.

(Smith & Nephew, UK). After the 6-DOF motion of the arthroscope was recorded, we determined whether the arthroscope moved within the derived conical workspace using morphological data.

Fig. 13 shows one of the recorded data and the conical workspace. The black points and the cone represent the recorded end tip position of the arthroscope and the minimum bounding conical workspace that contains the points, respectively. The minimum bounding cone was derived by modifying the minimum bounding sphere algorithm [29].

Fig. 14 (a) shows the results of measuring the movement of the arthroscope during the arthroscopic examinations through the PP. The horizontal axes in the plots represent the time in seconds, and the vertical axis in the upper plot indicates the angle between the longitudinal vector of the arthroscope and the z-axis of the portal coordinate (α in Fig. 14 (a)). The vertical axis of the lower plot represents the translationally moved displacement (d in Fig. 14 (a)). The orange dashed lines represent the maximum values of α and d. Fig. 14 (b) displays the results of Fig. 14 (a) as a probability density function. The blue dashed lines indicate the 95^{th} percentiles of α and d; the 95% of the times the arthroscope was located within a conical range of motion with the vertex angle α and d. Fig. 15 (a) shows the results of measuring the movement

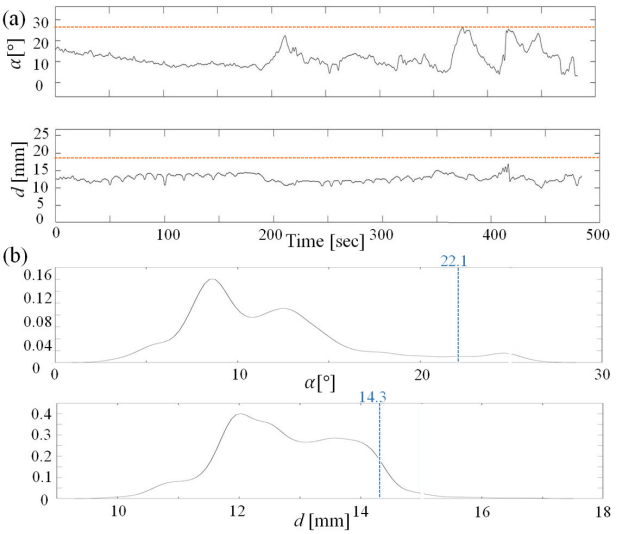

FIGURE 15. (a) α and d in time domain, (b) probability density of α and d during rotator cuff repair through LP.

of the arthroscope during rotator cuff repair through the LP. Fig. 15 (b) displays the results of Fig. 15 (a) as a probability density function. Each axis and dashed line of Fig. 15 have the same notations as shown in Fig. 14. The same experiment was repeated thrice by the two surgeons for arthroscopic examination and the three surgeons for rotator cuff repair, and the maximum α and maximum d are presented in Fig. 16 and Fig. 17, respectively. The 95^{th} percentiles of α and d are presented in the figures as well. The orange dashed lines indicate the theoretical maximum values of α and d (TABLE 3). The circled numbers represent each operator who participated in the experiment (e.g., ① is surgeon 1). The distributions of the experimental results are summarized in TABLE 5.

VI. DISCUSSION

In Fig. 10 and Fig. 11, the small teeth shape and large teeth shape appear alternately. Because they show the results of substituting the morphological data of TABLE 2 into (1), (3), (16), and (18) using the "for" statement in the order specified in the table (from *HHD* to d_{cg}), the morphological data affected the workspace in the same order. In the graph, the first 256 cases are the values substituted with $HHD = 45.7 - 3.2mm$, and the latter 256 cases are the values substituted with $HHD = 45.7 + 3.2mm$. On the other hand, the influence of d_{cg} appears alternately for all cases. The parameters that caused a large change in the graph were *HHD*, G_s, and G_l, that is, the morphological data that had a substantial influence on the derived workspace were the humeral head diameter (*HHD*) and glenoid size (G_s and G_l), which were directly related to the target point to be observed using the arthroscope. The parameters that caused only a minimal change in the graph were d_{cg}, *CP*, d_{roof}, *CSA*, t_{ac}, and *SAS*. The parameters that determine the location of the portal (d_{cg}, *CP*, d_{roof}, *CSA*, t_{ac}, and *SAS*) are those that have a minimal effect on workspace derivation. Therefore, the workspace

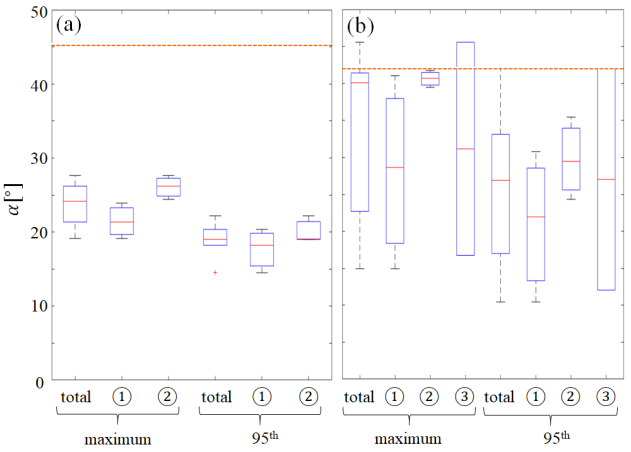

FIGURE 16. Box plot of α during (a) arthroscopic examination through PP and (b) rotator cuff repair through LP.

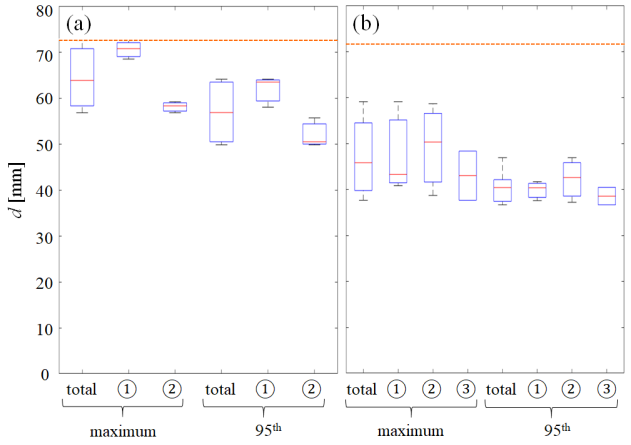

FIGURE 17. Box plot of d during (a) arthroscopic examination through PP and (b) rotator cuff repair through LP.

TABLE 5. Distribution of α and d.

portal	DOF	percentile	surgeon 1	surgeon 2	surgeon 3	total
posterior	α[°]	maximum	21.5±2.4	26.1±1.6	-	23.8±3.1
		95^{th}	17.7±3.0	20.1±1.8	-	18.9±2.6
	d[mm]	maximum	70.5±2.0	58.1±1.2	-	64.3±7.0
		95^{th}	61.8±3.4	52.0±3.2	-	56.9±6.1
lateral	α[°]	maximum	28.2±13.1	40.6±1.1	31.2±20.4	33.6±12.0
		95^{th}	21.1±10.2	29.7±5.6	27.0±21.2	25.8±10.9
	d[mm]	maximum	47.7±9.9	49.2±10.0	43.0±7.6	47.1±8.5
		95^{th}	39.8±2.1	42.2±4.8	38.5±2.7	40.4±3.4

of the arthroscope is largely determined by the parameters that determine the target point to be observed through the arthroscope, rather than the morphological parameters that determine the location of the portal. In addition, since we derived the workspace using the maximum value of α and d to incorporate all of these variations, it can be considered that the workspace that encompasses all the aforementioned variations was derived.

During the arthroscopic examination and rotator cuff repair of the shoulder joint of the cadaver, the arthroscope generally moves within its theoretical workspace, as summarized in TABLE 3 and TABLE 5. However, some of the maximum

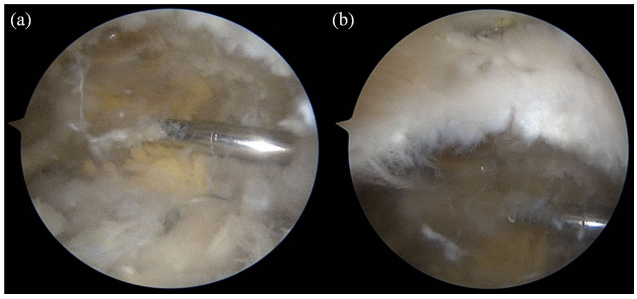

FIGURE 18. Arthroscopic screen when (a) arthroscope is targeting subacromial space, (b) arthroscope goes beyond theoretical workspace.

values of α when the arthroscope moves through the LP are greater than the theoretical value as depicted in Fig. 16 (b). This finding suggests that there is motion in which the arthroscope leaves the derived workspace, owing to the use of various surgical tools with both hands during rotator cuff repair. The actual α exceeds the theoretical maximum α because the arthroscope points the upper side of the SAS during rotator cuff repair, as shown in Fig. 18. Because the upper side of the SAS is a spot that does not need to be observed during rotator cuff repair, it can be excluded from the required workspace.

It can be seen that the α value measured during rotator cuff repair is more dispersed for each trial than other values are (Fig. 16 (b)). Even when one operator performs the same rotator cuff repair several times, the vertex angle of workspace varies considerably because the surgery is performed using not only the arthroscope but also other surgical instruments during the rotator cuff repair, which includes numerous unnecessary movements. The surgeon needed more than two hands during the rotator cuff repair; thus, there was unnecessary movement while passing the arthroscope to the assistant. In Fig. 16 (b), the values exceed the maximum α value of the derived workspace (orange dashed line) due to the unnecessary movement, thus, they are negligible. It can be also seen that the d value measured during arthroscopic examination through the PP is almost constant for each trial. However, there is significant difference among the operators (Fig. 17 (a)). Even if the same affected area is observed in arthroscopic examination, the depth of the arthroscopic insertion is different for each operator, because the degree of zoom in/out desired for each operator is different even in the same surgical situation. However, for all trials conducted by various operators, there was no case where the actual d value exceeded the d value of the derived workspace (orange dashed line). Thus, the derived workspace can be considered feasible.

The 95^{th} percentiles in Fig. 16 and Fig. 17 indicate that 95% of the time, the arthroscope was located within a conical workspace having the vertex angle of the α value and slant height of the d value. Specifically, because the 95^{th} percentile represents the predominant location of the arthroscope, it can be regarded as a workspace in which nonessential motion is excluded. Because the 95^{th} percentiles of α and d are

smaller than the corresponding theoretical maximum values, it is confirmed that the workspace of the arthroscope that was previously obtained theoretically is feasible.

When using the proposed method, it is expected that there will be errors in the formulas of the locations of the landmarks, owing to simplification of the complex shape of the shoulder anatomy as a simple geometric model. For example, the humeral head and shoulder surface are assumed to be perfect spheres, and the acromion arch is assumed to be a complete arch. It is also assumed that the glenoid is a perfect ellipse. The bones in the human body are not perfect ovals or arches; thus several errors will exist in the workspace derivation. However, these assumptions are reliable because they have already been applied in the medical morphology field [20]–[25], and the number of errors appears to decrease as the sample size increases. The workspace measurement in the cadaveric test revealed that the simplification was reliable because the arthroscope showed its movement in the derived workspace.

Since the arthroscope moves within a narrow affected area, care must be taken not to injure the human tissues such as cartilage or ligaments. A limitation of this study is that a safety function was not incorporated into the robotic arthroscope manipulator (Fig. 1) to prevent human injury. This limitation can be addressed by measuring or estimating the contact force of the end effector of a surgical robot [30]–[32].

Because the proposed workspace derivation method utilizes morphological measurement data, it is easy to secure a large sample size. In this study, the measured morphological data [20]–[25] were employed; thus, the sample size could be at least 70 without additional time and cost. In addition, by using $\bar{x} - s$ and $\bar{x} + s$ for each parameter of morphological data, it was possible to derive a workspace that can cope with the variation of various patients. Another advantage of the proposed method is that because a geometric model is utilized, the workspace for other tasks in shoulder arthroscopy rather than rotator cuff repair can be easily derived.

VII. CONCLUSION

In this study, we proposed a method for deriving the workspace of an arthroscope using morphological data for arthroscopic rotator cuff repair surgery. For simplified modeling, the humeral head and shoulder surface were assumed to be spheres, and the glenoid plane was assumed to be an ellipse. In addition, the three-dimensional positions of the ALA, PLA, and LA were determined using morphological measurements. Based on these criteria, the positions of the anterior, posterior, and lateral portals were determined using the standard portal placement method. We obtained a conical workspace that the arthroscope should reach through each portal during arthroscopic examination and rotator cuff repair surgery. For evaluation, the workspace of an arthroscope during arthroscopic examination and rotator cuff repair was measured through a cadaveric test and was compared with the theoretical workspace. The derived workspace of the arthroscope was found to be feasible.

This research proposed a theoretical workspace for arthroscopic examination and rotator cuff repair using morphological data of the shoulder joint. The morphological data contained information on a wide variety of shoulder joints; therefore, the workspace of the arthroscope that incorporates various shoulder joints could be derived without conducting numerous experiments. Accordingly, workspace analysis using this method will reduce the time and cost of the preliminary research phase. In addition, the derived theoretical model of the shoulder joint can be applied to derive the workspace of the arthroscope required for various shoulder arthroscopies as well as rotator cuff repair. Furthermore, the model can be applied to various orthopedic fields rich in morphological data, such as knee joints and hip joints, using a similar method.

If the findings of this research are applied to a robotic arthroscope manipulator, the designs of the active robotic arm and positioning arm can be optimized. The optimal base point of the robotic system for reaching the workspace required for the target procedure can also be derived. If the results of this study are employed for path planning of a robotic arthroscope manipulator, the path of the end effector can be planned by defining the target point and obstacles to be avoided. For example, using the geometric model of the portal location, humeral head, and glenoid, the path of the arthroscope tip can be planned to pass through the affected area while avoiding a collision between the arthroscope and the humeral head/glenoid.

In a future study, we will design a robotic arthroscope manipulator optimized for the proposed workspace, as shown in Fig. 1. We will then use this manipulator to perform arthroscopic rotator cuff repair and verify its feasibility in actual operation.

APPENDIX

ABBREVIATIONS

Anatomical designation	Abbreviation
Radius of shoulder [mm]	r_s
Humeral Head Diameter [mm]	*HHD*
Sub Acromial Space [mm]	*SAS*
Acromion thickness [mm]	t_{ac}
Major (longer) axis of glenoid [mm]	G_l
Minor (shorter) axis of glenoid [mm]	G_s
Critical Shoulder Angle [°]	*CSA*
Lateral acromial roof extension [mm]	d_{roof}
Coracoid process Prominence [mm]	CP
Distance between coracoid process tip and uppermost point of glenoid [mm]	d_{cg}
Anterolateral tip of acromion	ALA
Posterolateral tip of acromion	PLA
Lateral tip of acromion	LA
Coracoid Process Tip	CPT
Anterior Portal	AP
Posterior Portal	PP
Lateral Portal	LP

REFERENCES

[1] K. T. den Boer, J. Dankelman, D. J. Gouma, and H. G. Stassen, "Peroperative analysis of the surgical procedure," *Surgical Endoscopy Other Interventional Techn.*, vol. 16, no. 3, pp. 492–499, Mar. 2002.

[2] L. Mettler, M. Ibrahim, and W. Jonat, "One year of experience working with the aid of a robotic assistant (the voice-controlled optic holder AESOP) in gynaecological endoscopic surgery," *Hum. Reproduction*, vol. 13, no. 10, pp. 2748–2750, Oct. 1998.

[3] C. A. Nelson, X. Zhang, B. C. Shah, M. R. Goede, and D. Oleynikov, "Multipurpose surgical robot as a laparoscope assistant," *Surgical Endoscopy*, vol. 24, no. 7, pp. 1528–1532, Jul. 2010.

[4] W. Lin, D. Navarro-Alarcon, P. Li, Z. Wang, H. M. Yip, Y.-H. Liu, and M. C. F. Tong, "Modeling, design and control of an endoscope manipulator for FESS," in *Proc. IEEE/RSJ Int. Conf. Intell. Robots Syst. (IROS)*, Sep. 2015, pp. 811–816.

[5] J. Gilbert, "The EndoAssist robotic camera holder as an aid to the introduction of laparoscopic colorectal surgery," *Ann. Roy. College Surgeons England*, vol. 91, no. 5, pp. 389–393, Jul. 2009.

[6] B. Herman, K. T. Duy, B. Dehez, R. Polet, B. Raucent, E. Dombre, and J. Donnez, "Development and first *in vivo* trial of EvoLap, an active laparoscope positioner," *J. Minimally Invasive Gynecol.*, vol. 16, no. 3, pp. 344–349, May 2009.

[7] S. Y. Ko, J. Kim, W. J. Lee, and D. S. Kwon, "Compact laparoscopic assistant robot using a bending mechanism," *Adv. Robot.*, vol. 21, nos. 5–6, pp. 689–709, 2007.

[8] D.-H. Kang, H.-W. Baek, B.-S. Cheon, D.-G. Jeong, H.-Y. Lee, and D.-S. Kwon, "Robotic handler for interchangeability with various size of laparoscope," in *Proc. 13th Int. Conf. Ubiquitous Robots Ambient Intell. (URAI)*, Aug. 2016, pp. 21–25.

[9] J.-U. Stolzenburg, T. Franz, P. Kallidonis, D. Minh, A. Dietel, J. Hicks, M. Nicolaus, A. Al-Aown, and E. Liatsikos, "Comparison of the FreeHand robotic camera holder with human assistants during endoscopic extraperitoneal radical prostatectomy," *BJU Int.*, vol. 107, no. 6, pp. 970–974, Mar. 2011.

[10] P. J. Berkelman, P. Cinquin, J. Troccaz, J.-M. Ayoubi, and C. Létoublon, "Development of a compact cable-driven laparoscopic endoscope manipulator," in *Proc. Int. Conf. Med. Image Comput. Comput.-Assist. Intervent.* Berlin, Germany: Springer, 2002.

[11] M. J. H. Lum, J. Rosen, M. N. Sinanan, and B. Hannaford, "Optimization of a spherical mechanism for a minimally invasive surgical robot: Theoretical and experimental approaches," *IEEE Trans. Biomed. Eng.*, vol. 53, no. 7, pp. 1440–1445, Jul. 2006.

[12] A. Faraz and S. Payandeh, "A robotic case study: Optimal design for laparoscopic positioning stands," *Int. J. Robot. Res.*, vol. 17, no. 9, pp. 986–995, Sep. 1998.

[13] Q. C. Nguyen, Y. Kim, and H. Kwon, "Optimization of layout and path planning of surgical robotic system," *Int. J. Control, Autom. Syst.*, vol. 15, no. 1, pp. 375–384, Feb. 2017.

[14] S.-W. Son and D.-S. Kwon, "A convex programming approach to the base placement of a 6-DOF articulated robot with a spherical wrist," *Int. J. Adv. Manuf. Technol.*, vol. 102, nos. 9–12, pp. 3135–3150, 2019.

[15] C. Cao and C. L. MacKenzie, and S. Payandeh, "Task and motion analyses in endoscopic surgery," in *Proc. ASME Dyn. Syst. Control Division*, 1996, pp. 583–590.

[16] J. G. Person, A. J. Hodgson, and A. G. Nagy, "Automated high-frequency posture sampling for ergonomic assessment of laparoscopic surgery," *Surgical Endoscopy*, vol. 15, no. 9, pp. 997–1003, Sep. 2001.

[17] R. Riener, S. Reiter, M. Rasmus, D. Wetzel, and H. Feussner, "Acquisition of arm and instrument movements during laparoscopic interventions," *Minimally Invasive Therapy Allied Technol.*, vol. 12, no. 5, pp. 235–240, Jan. 2003.

[18] J. Rosen, "The blue dragon-a system for monitoring the kinematics and the dynamics of endoscopic tools in minimally invasive surgery for objective laparoscopic skill assessment," in *Proc. Stud. Health Technol. Informat.*, Jan. 2002, pp. 412–418.

[19] A. Soroush and F. Farahmand, "Workspace measurement of the surgeon's upper limb during an arthroscopy and three laparoscopy operations using inertial sensor systems," in *Proc. E-Health Bioeng. Conf. (EHB)*, Nov. 2013, pp. 1–4.

[20] G. R. Milner and J. L. Boldsen, "Humeral and femoral head diameters in recent white American skeletons," *J. Forensic Sci.*, vol. 57, no. 1, pp. 35–40, Jan. 2012.

[21] C. J. Petersson and I. Redlund-Johnell, "The subacromial space in normal shoulder radiographs," *Acta Orthopaedica Scandinavica*, vol. 55, no. 1, pp. 57–58, Jan. 1984.

[22] W. A. N. El-Din, "A morphometric study of the patterns and variations of the acromion and glenoid cavity of the scapulae in Egyptian population," *J. Clin. Diagnostic Res.*, vol. 9, no. 8, p. AC08, 2015.

[23] W. Chaijaroonkhanarak, P. Amarttayakong, S. Ratanasuwan, P. Kirirat, W. Pannangrong, J. U. Welbat, P. Prachaney, A. Chaichun, and S. Sae-Jung, "Predetermining glenoid dimensions using the scapular dimensions," *Eur. J. Orthopaedic Surgery Traumatol.*, vol. 29, no. 3, pp. 559–565, Apr. 2019.

[24] S. Beeler, A. Hasler, T. Götschi, D. C. Meyer, and C. Gerber, "Critical shoulder angle: Acromial coverage is more relevant than glenoid inclination," *J. Orthopaedic Res.*, vol. 37, no. 1, pp. 205–210, Jan. 2019.

[25] S. Gumina, F. Postacchini, L. Orsina, and G. Cinotti, "The morphometry of the coracoid process–its aetiologic role in subcoracoid impingement syndrome," *Int. Orthopaedics*, vol. 23, no. 4, pp. 198–201, Nov. 1999.

[26] R. Prejbeanu, I. B. Codorean, and S. Tanase, "Shoulder arthroscopy: General setup, portal options, and how to manage a complete shoulder investigation," in *Arthroscopy*. Berlin, Germany: Springer, 2016, pp. 421–429.

[27] S. J. Snyder, "Diagnostic arthroscopy of the shoulder. Normal anatomy and variations," in *Shoulder Arthroscopy*. Philadelphia, PA, USA: Lippincott Williams & Wilkins, 2003, pp. 22–38.

[28] P. Boileau, N. Brassart, D. J. Watkinson, M. Carles, A. M. Hatzidakis, and S. G. Krishnan, "Arthroscopic repair of full-thickness tears of the supraspinatus: Does the tendon really heal?" *JBJS*, vol. 87, no. 6, pp. 1229–1240, 2005.

[29] A. Semechko. (2020). *Exact Minimum Bounding Spheres and Circles*. GitHub. Accessed: Aug. 19, 2020. [Online]. Available: https://github.com/AntonSemechko/Bounding-Spheres-And-Circles

[30] S. Shimachi, S. Hirunyanitiwatna, Y. Fujiwara, A. Hashimoto, and Y. Hakozaki, "Adapter for contact force sensing of the da Vinci robot," *Int. J. Med. Robot. Comput. Assist. Surgery*, vol. 4, no. 2, pp. 121–130, Jun. 2008.

[31] N. Yilmaz, J. Y. Wu, P. Kazanzides, and U. Tumerdem, "Neural network based inverse dynamics identification and external force estimation on the da Vinci Research Kit," in *Proc. IEEE Int. Conf. Robot. Autom. (ICRA)*, May 2020, pp. 1387–1393.

[32] Z. Chua, A. M. Jarc, and A. M. Okamura, "Toward force estimation in robot-assisted surgery using deep learning with vision and robot state," 2020, *arXiv:2011.02112*. [Online]. Available: http://arxiv.org/abs/2011.02112

CHANG-KYUN KIM received the B.S. degree from the Department of Mechanical Engineering, Korea Advanced Institute of Science and Technology (KAIST), Daejeon, South Korea, in 2017, where he is currently pursuing the integrated master's and Ph.D. degree program. His research interests include mechanism design, surgical robotics, and medical devices.

JOONHWAN KIM received the B.S. degree in mechanical engineering from Kyushu University, Fukuoka, Japan, in 2012, and the M.S. and Ph.D. degrees in bioengineering from The University of Tokyo, Tokyo, Japan, in 2014 and 2018, respectively. He is currently working as a Postdoctoral Researcher with the Human-Robot Interaction Research Center, Korea Advanced Institute of Science and Technology, Daejeon, Republic of Korea. His research interests include surgical robotics and human–robot interaction.

DONGJUN PARK received the B.S. degree from the Department of Medicine, Konyang University, Daejeon, South Korea, in 2011, and the M.S. degree from the Department of Medicine, Inje University, Busan, South Korea, in 2019. From 2015 to 2019, he received resident training with the Department of Orthopaedic Surgery, Ilsanpaik Hospital. He trained fellowship with the Department of Orthopaedic Surgery, Asan Medical Center, Seoul, South Korea, in 2019. He is a specialist of shoulder and elbow as an Orthopaedic Surgery Medical Doctor. He is currently a Medical Doctor with the Department of Orthopaedic Surgery, Ilsanpaik Hospital.

DONG-SOO KWON (Senior Member, IEEE) received the B.S. degree from the Department of M.E., Seoul National University, South Korea, in 1980, the M.S. degree from the Department of M.E., Korea Advanced Institute of Science and Technology (KAIST), in 1982, and the Ph.D. degree from the Department of M.E., Georgia Institute of Technology, in 1991. From 1991 to 1995, he worked as a Research Staff with the Telerobotics Section, Oak Ridge National Laboratory. From 2008 to 2009, he was a Visiting Professor with the Department of M.E., Georgia Institute of Technology. He is currently a Professor with the Department of Mechanical Engineering, KAIST. He is also the Director of the Human–Robot Interaction Research Center, KAIST, and the Center for Future Medical Robotics. He is the CEO of EasyEndo Surgical Inc., a President of the Robot Convergence Forum, South Korea, the Chairman of Board of Directors of the Korea Institute of Robot and Convergence, and a member of the National Academy of Engineering of Korea. His research interests include human–robot interaction, medical robotics, telerobotics, and haptics.